Particuology xxx (2016) xxx–xxx

Contents lists available at ScienceDirect

Particuology

journal homepage: www.elsevier.com/locate/partic

In situ and ex situ synthesis of poly(vinyl alcohol)–Fe_3O_4 nanocomposite flame retardants

Davood Ghanbari [a], Masoud Salavati-Niasari [b,*], Majid Ghasemi-Kooch [b]

[a] Young Researchers and Elite Club, Arak Branch, Islamic Azad University, Arak, Iran
[b] Institute of Nano Science and Nano Technology, University of Kashan, PO Box 87317-51167, Kashan, Iran

ARTICLE INFO

Article history:
Received 3 April 2015
Received in revised form
24 November 2015
Accepted 6 December 2015
Available online xxx

Keywords:
Nanocomposite
Polymer
Magnetite
Precipitation
Thermal stability
Flame retardancy

ABSTRACT

Application of flame retardants is limited because of environmental requirements. This work introduces conventional magnetic nanoparticles as a new class of nontoxic and effective flame retardant. Fe_3O_4 enhanced both the thermal stability and flame retardant properties of a poly(vinyl alcohol) matrix. Nanoparticles were synthesized via a simple precipitation reaction without using an inert atmosphere at room temperature. The effects of different precursors and acrylamide on the morphology of the products were investigated. Nanoparticles exhibited a ferrimagnetic behavior at room temperature. To prepare the magnetic nanocomposite, Fe_3O_4 nanoparticles were added to the poly(vinyl alcohol). In the presence of a flame, the magnetic nanoparticles remained together, showed resistance to dripping and protected the polymer matrix. Dispersed nanoparticles play a role of a magnetic barrier layer, which slows product volatilization and prevents flames and oxygen from reaching the sample during decomposition of the polymer.

Introduction

Magnetic nanomaterials have attracted attention in various applications such as the absorption of microwave radiation, clinical diagnosis, mineral separation, magneto-optic materials, magnetic storage devices, and microwave filters. Magnetite (Fe_3O_4) exhibits unique electric and magnetic properties because of the transfer of electrons between Fe^{2+} and Fe^{3+} in the octahedral sites. Because of their biocompatibility, low toxicity, and adjustable magnetic properties, Fe_3O_4 have received considerable attention in various areas such as drug targeting, cancer therapy, magnetic cell separation, enzyme immobilization catalysis, magnetic refrigeration systems, and heat transfer applications (Ghanbari, Salavati-Niasari, & Ghasemi-Kooch, 2014; Gholamian, Salavati-Niasari, Ghanbari, & Sabet, 2013). Nanostructures have been intensively studied in a wide range of applications because the properties of nanocrystals depend on their composition, shape, size, structure, phase, and size distribution. The reactivity and selectivity of nanoparticles can be adjusted by controlling the morphology because the exposed surfaces of the particles have distinct crystallographic planes depending on the shape (Ghanbari, Salavati-Niasari, & Sabet, 2012; Kuljanin, Čomor, Djoković, & Nedeljković, 2006; Morgan & Wilkie, 2007; Sun & Xiang, 2008; Wang, Liu, & Wang, 2010). Polymeric nanocomposites have gained much attention because adding a small amount of nanoparticles to a polymeric matrix can lead to improving the properties of the matrix. The principal benefits of these compounds over many metallic alloys are corrosion resistance, low density, and thermal insulation. However, the main disadvantage of polymeric compounds is high flammability (Grigsby, Ferguson, Franich, & Russell, 2005; Henrist, Mathieu, Vogels, Rulmont, & Cloots, 2003; Karunakaran, Dhanalakshmi, & Gomathisankar, 2010; Laoutid, Bonnaud, Alexandre, Lopez-Cuesta, & Dubois, 2009; Wang, Fang, Chen, & Wang, 2007). Conventional flame retardants such as halogenated and aromatic compounds are toxic and restricted because of environmental controls (Beyer, 2001; Franco, Nassar, & Cortés, 2014; Liu, Ying, Zhou, & Xie, 2009; Wu, Shao, Gu, & Wei, 2004). We report the precipitation synthesis of Fe_3O_4 nanoparticles and poly(vinyl alcohol) (PVA)–Fe_3O_4 nanocomposites using $FeCl_2$ as a single precursor. The synthesis at normal conditions without using an inert atmosphere is a novelty of this work. Nanoparticles enhanced the thermal stability and flame retardancy of the PVA matrix. By distributing Fe_3O_4 into PVA, nanocomposites' coercivity was also increased. The nanostructures were characterized using scanning electron microscopy

* Corresponding author. Tel.: +98 31 55912383; fax: +98 31 55913201.
E-mail address: salavati@kashanu.ac.ir (M. Salavati-Niasari).

http://dx.doi.org/10.1016/j.partic.2015.12.003

(SEM), transmission electron microscopy (TEM), X-ray diffraction (XRD), energy dispersive X-ray spectroscopy (EDS), Fourier transform infrared spectroscopy (FTIR), and atomic force microscopy (AFM).

Experimental

Materials and instruments

$FeCl_2{\cdot}4H_2O$, $FeCl_3{\cdot}6H_2O$, PVA (MW: 20,000–30,000), NH_3, and NaOH were purchased from Merck Company. All of the chemicals were used as received without further purifications. XRD patterns were recorded by an X-ray diffractometer (Philips, the Netherlands) using Ni-filtered Cu Kα radiation. SEM images were obtained using an instrument model 1455VP (LEO, Germany). Prior to taking images, the samples were coated by a very thin layer of Pt to make the sample surface conductive and prevent charge accumulation, obtaining a better contrast. The magnetic properties of the samples were determined at room temperature using a vibrating sample magnetometer (VSM, Meghnatis

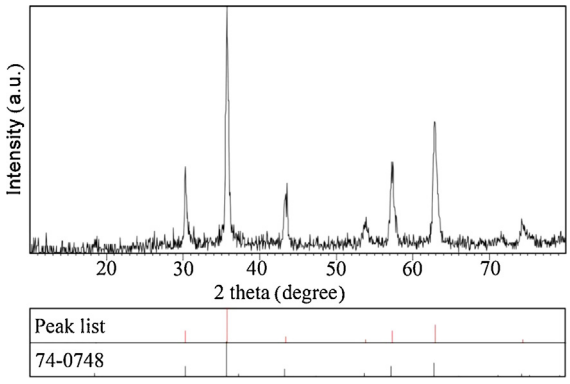

Fig. 1. XRD pattern of the Fe_3O_4 nanoparticles.

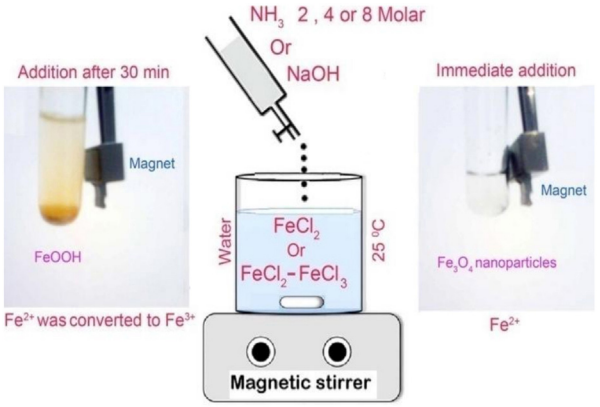

Fig. 3. Fe_3O_4 preparation and magnetic comparison of the obtained products of NH_3 addition immediately or after 30 min.

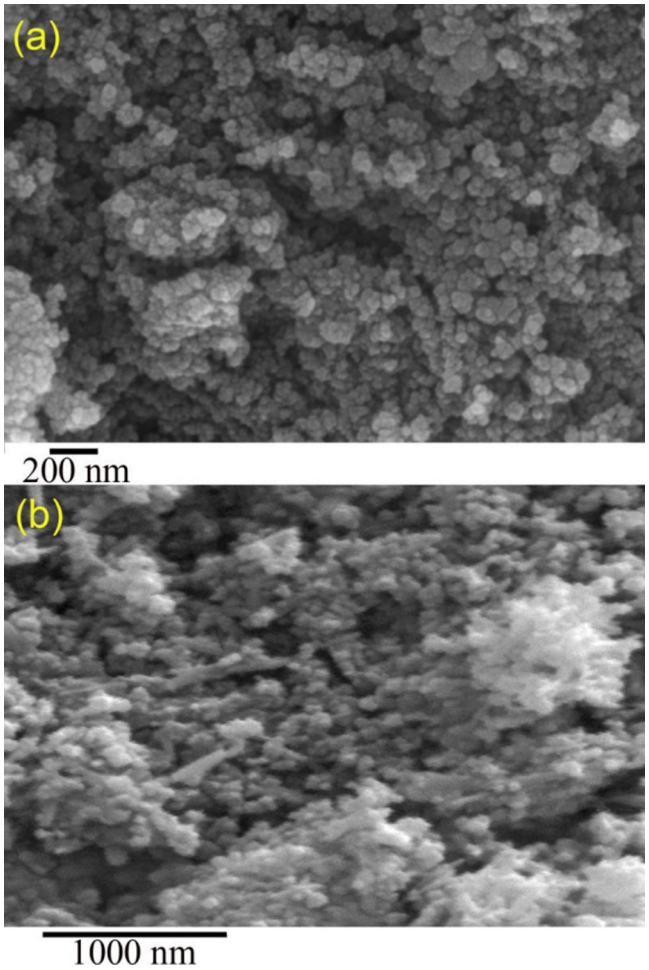

Fig. 2. SEM images of Fe_3O_4 nanoparticles achieved by $FeCl_2$ (a) with and (b) without acrylamide.

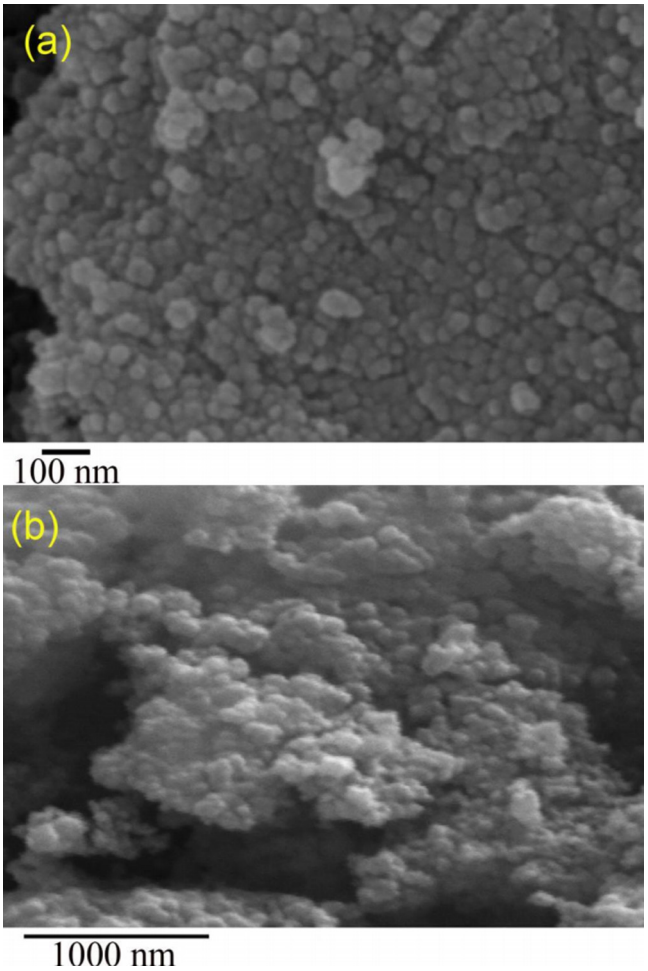

Fig. 4. Fe_3O_4 nanoparticles synthesized using $FeCl_2$–$FeCl_3$ (a) with and (b) without acrylamide.

Please cite this article in press as: Ghanbari, D., et al. In situ and ex situ synthesis of poly(vinyl alcohol)–Fe_3O_4 nanocomposite flame retardants. *Particuology* (2016), http://dx.doi.org/10.1016/j.partic.2015.12.003

Kavir Kashan Co., Kashan, Iran). Thermogravimetric analysis (TGA) was carried out using an instrument (TGA-50H, Shimadzu, Japan) with a heating rate of 10 °C/min under a nitrogen atmosphere. A multiwave ultrasonic generator (MS 72, Bandeline, Germany), equipped with a converter/transducer and titanium oscillator, operating at 20 kHz with a maximum power output of 76 W was used for the dispersion of nanoparticles. In the UL-94 test, a bar shape sample 130 mm × 13 mm × 1.6 mm was held vertically, and a Bunsen burner flame was applied to the specimen twice (10 s each). TEM images were obtained on a Philips EM208 TEM with an accelerating voltage of 100 kV.

Synthesis of Fe_3O_4 nanoparticles

$FeCl_2$ (2.57 g, with or without 0.5 g acrylamide) was dissolved in 100 mL of distilled water. A 50-mL amount of NH_3 (2 M) solution was then slowly added to the solution. A black precipitate was obtained, confirming the synthesis of Fe_3O_4. The precipitate of Fe_3O_4 was centrifuged and rinsed with distilled water, and dried in an atmosphere environment.

Ex situ synthesis of PVA–Fe_3O_4 nanocomposites

PVA (4 g) was dissolved in 10 mL of water, and Fe_3O_4 (1 g) was dispersed in 10 mL of water with ultrasonic treatment (30 min, 60 W). The dispersion of Fe_3O_4 was added slowly to the polymer solution. The solution was mixed under stirring for 10 h at ambient temperature. For the preparation of samples for the UL-94 test, the product was cast on a template with the dimensions 130 mm × 13 mm, and after 48 h of solvent evaporation, the nanocomposite was placed in a vacuum oven for another 10 h to remove residual traces of water. The final specimens for the test were 130 mm × 13 mm × 1.6 mm.

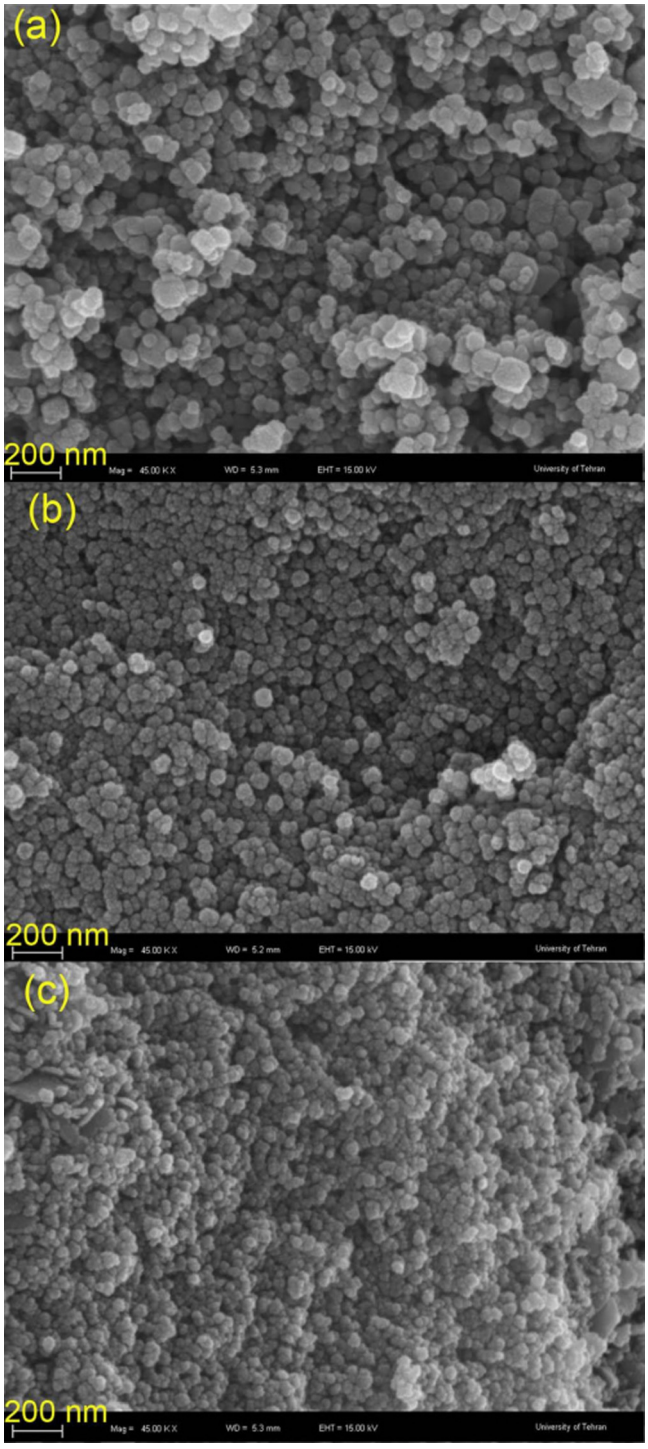

Fig. 5. Fe_3O_4 nanoparticles obtained by (a) NaOH, (b) NH_3 4 M, or (c) NH_3 8 M.

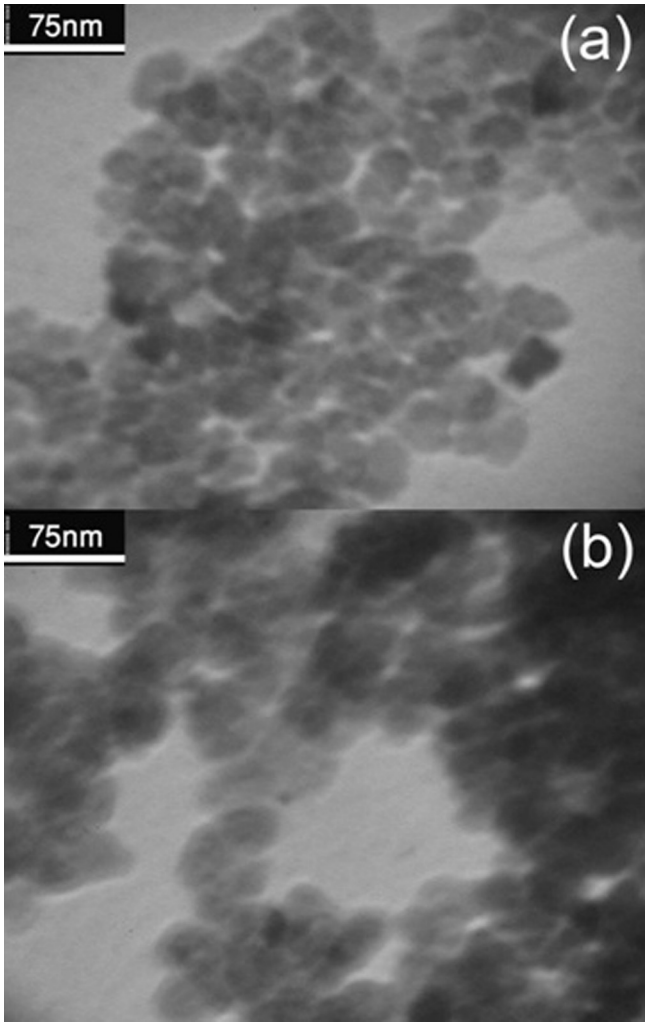

Fig. 6. TEM images of Fe_3O_4 nanoparticles synthesized with (a) $FeCl_2$ alone and (b) $FeCl_2$–$FeCl_3$.

Please cite this article in press as: Ghanbari, D., et al. In situ and ex situ synthesis of poly(vinyl alcohol)–Fe_3O_4 nanocomposite flame retardants. Particuology (2016), http://dx.doi.org/10.1016/j.partic.2015.12.003

In situ synthesis of PVA–Fe_3O_4 nanocomposites

PVA (4 g) and $FeCl_2$ (2.57 g) were dissolved in 15 mL of water, and NH_3 was added to the solution. The solution was mixed under stirring for 10 h at ambient temperature. For the preparation of samples for the UL-94 test, the product was cast with the dimensions 130 mm × 13 mm, and after 48 h of water evaporation, the nanocomposite was placed in a vacuum oven for 10 h to remove residual traces of solvents.

Results and discussion

The XRD pattern of Fe_3O_4 nanoparticles is shown in Fig. 1. The pattern of as-prepared Fe_3O_4 nanoparticles is indexed as a pure cubic phase (space group: $Fd\bar{3}m$), which is concordant with the literature values (JCPDS No. 74-0748). The narrow sharp peaks indicate that the Fe_3O_4 nanoparticles are well crystallized.

The crystallite size measurements were carried out using the Scherrer equation, $D_c = K\lambda/\beta\cos\theta$, where, β is the width of the observed diffraction peak at its half maximum intensity, K is the so-called shape factor, which usually takes a value of about 0.9, and

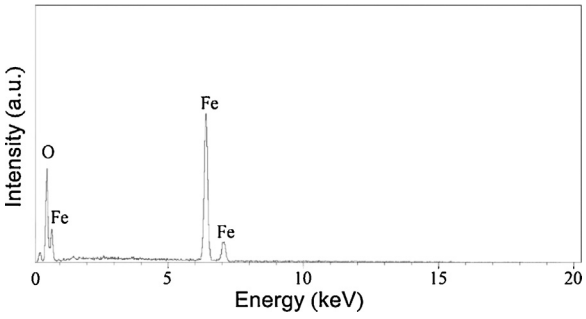

Fig. 7. EDS analysis of Fe_3O_4 nanoparticles.

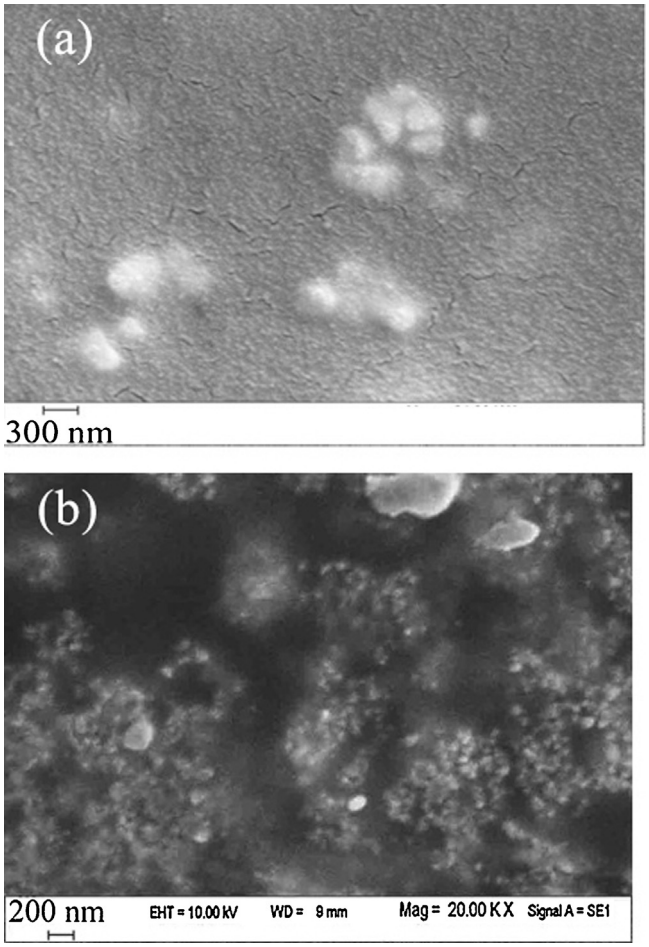

Fig. 8. SEM image of (a) the in situ-synthesized and (b) the ex situ-synthesized PVA–Fe_3O_4 nanocomposites.

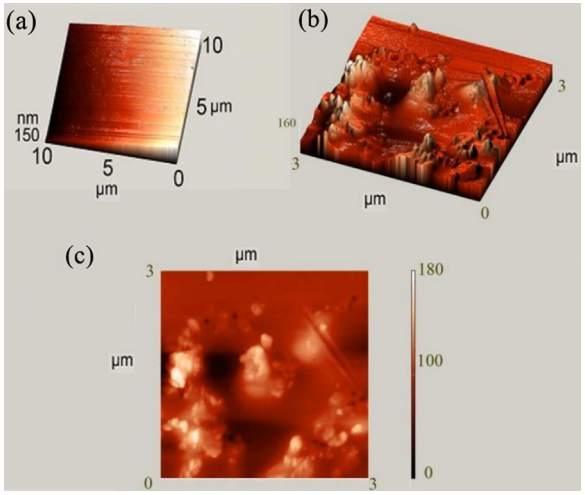

Fig. 9. Topographic images forming by AFM of (a) pure PVA and (b, c) the synthesized PVA–Fe_3O_4 nanocomposite.

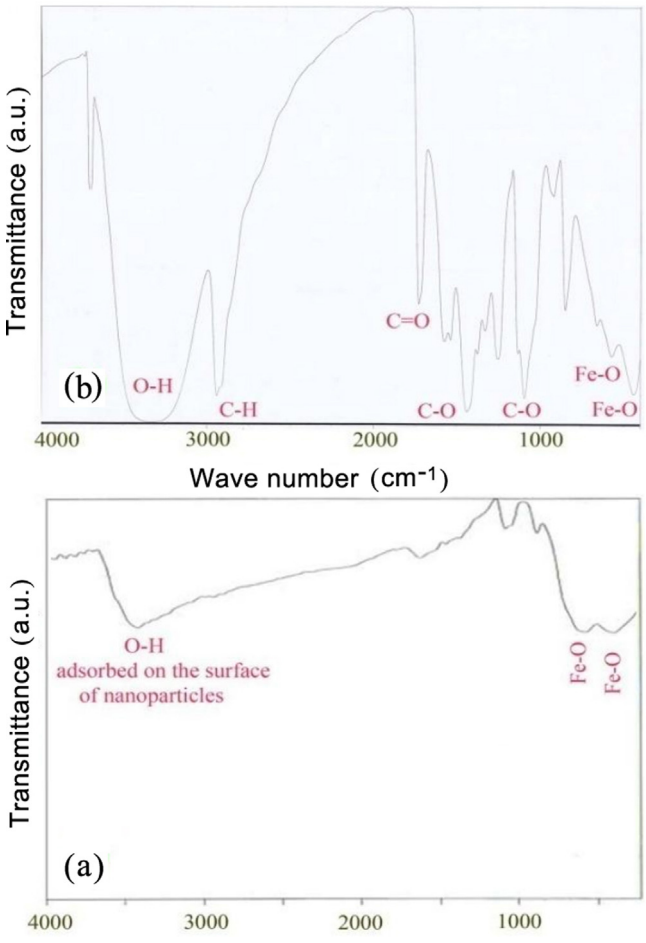

Fig. 10. FT-IR spectra of (a) Fe_3O_4 nanoparticles and (b) PVA–Fe_3O_4 nanocomposite.

Please cite this article in press as: Ghanbari, D., et al. In situ and ex situ synthesis of poly(vinyl alcohol)–Fe_3O_4 nanocomposite flame retardants. *Particuology* (2016), http://dx.doi.org/10.1016/j.partic.2015.12.003

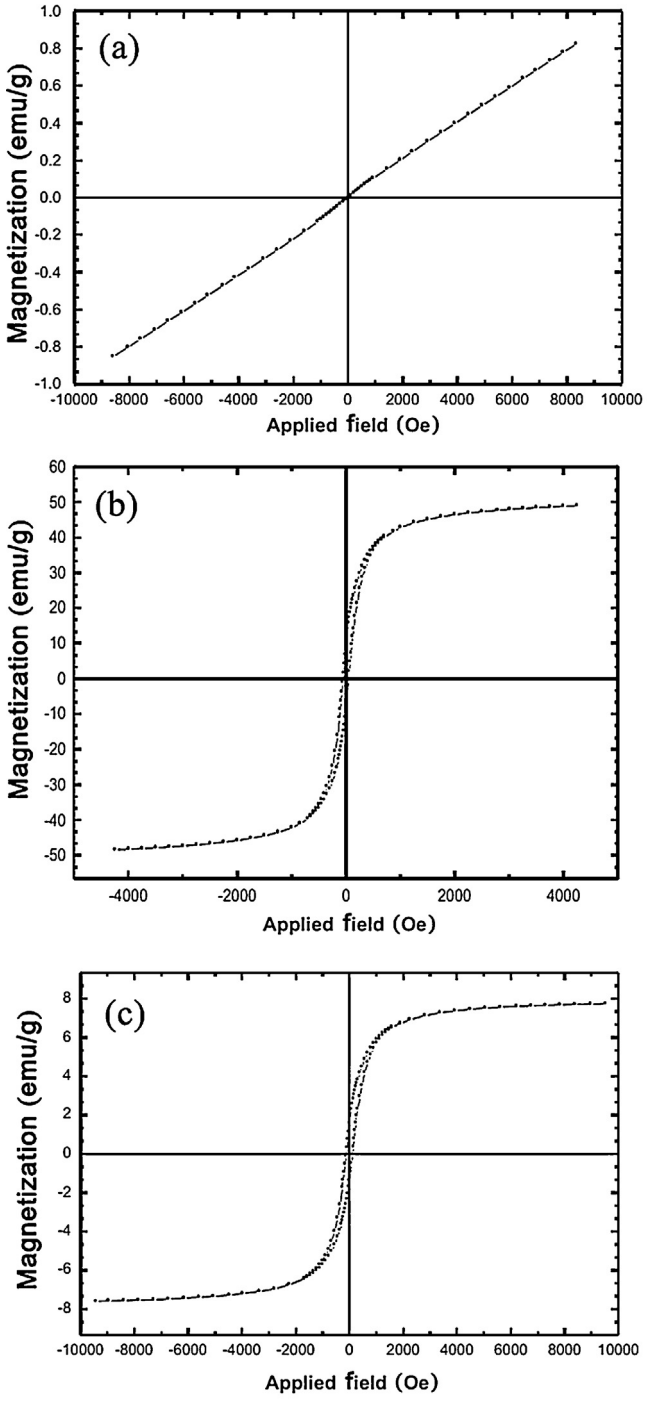

Fig. 11. Magnetization curves of (a) FeOOH product, (b) Fe_3O_4 nanoparticles, and (c) PVA–Fe_3O_4 nanocomposite.

λ is the X-ray wavelength (0.154 nm). The estimated crystallite size is about 14 nm.

The influence of acrylamide on the morphologies of the products is illustrated in Fig. 2. Using acrylamide in the nucleation stage leads to nanoparticles with a lower particle size.

If $FeCl_2$ remains in water more than 30 min before adding NH_3, most of the Fe^{2+} ions are oxidized to Fe^{3+} and brown FeOOH nanoparticles are obtained (Ghanbari et al., 2014). Immediately adding NH_3 results in the formation of pure black Fe_3O_4 nanoparticles. Comparison of magnetic properties of the products obtained at different NH_3 addition times is depicted in Fig. 3.

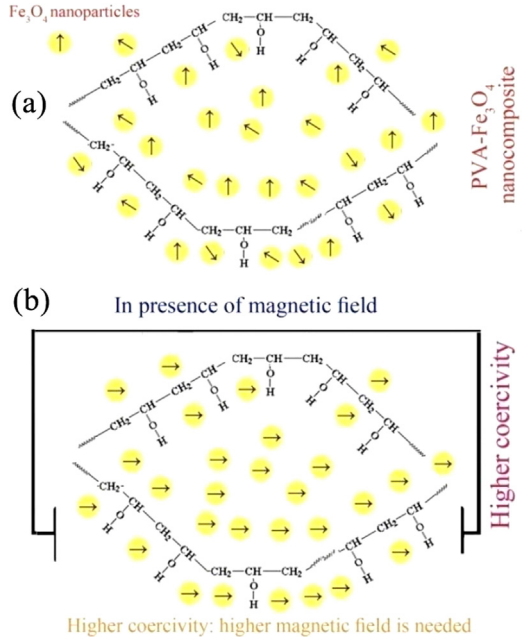

Fig. 12. (a) Fe_3O_4 nanoparticles distributed in the PVA matrix and (b) in the presence of a magnetic field.

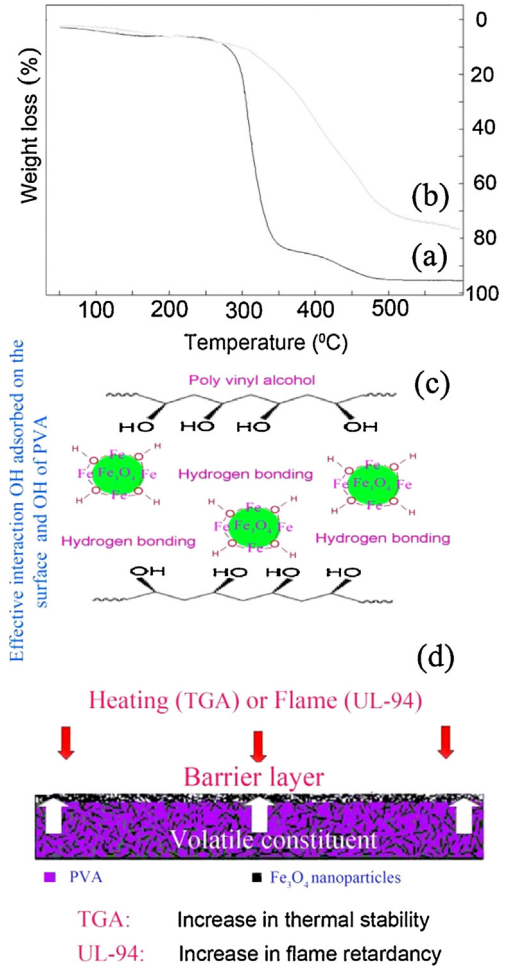

Fig. 13. TGA curves of (a) PVA and (b) PVA–Fe_3O_4 nanocomposite; (c) the interaction of Fe_3O_4 nanoparticles on the PVA surface; and (d) the nanocomposite performance against heat, oxygen and flame.

Please cite this article in press as: Ghanbari, D., et al. In situ and ex situ synthesis of poly(vinyl alcohol)–Fe_3O_4 nanocomposite flame retardants. *Particuology* (2016), http://dx.doi.org/10.1016/j.partic.2015.12.003

The preparation of the PVA–Fe_3O_4 nanocomposite is shown in Fig. 4. The SEM images of the product obtained by the $FeCl_2$–$FeCl_3$ precursor with and without acrylamide are illustrated in Fig. 4. In this case, $FeCl_3$ was dissolved first, then $FeCl_2$, and ammonia was added immediately to the solution. Fig. 4 shows that using acrylamide produces suitable monodisperse nanoparticles with a smaller particle size than those without acrylamide.

The effect of ammonia concentration and its replacement by sodium hydroxide is shown in Fig. 5. Fig. 6(a) shows the SEM image of Fe_3O_4 nanoparticles obtained with sodium hydroxide, and larger nanoparticles were achieved than those using ammonia. SEM images of the products obtained using ammonia at 4 and 8 M are shown in Fig. 5(b) and (c), respectively. The increased ammonia concentration led to agglomeration. The result indicates that a lower NH_3 concentration in the nucleation stage is a predominant factor in the growth stage, and smaller nanoparticles were produced. TEM images of the products obtained using acrylamide with $FeCl_2$ alone and $FeCl_2$–$FeCl_3$ are illustrated in Fig. 6(a) and (b), respectively. Monodisperse nanoparticles with an average diameter of 30 nm were obtained using acrylamide alone.

The chemical purity of the Fe_3O_4 nanoparticles was analyzed by EDS. Fig. 7 shows a representative EDS spectrum of the sample exhibiting only the peaks of Fe and O, suggesting there were no impurities.

Fig. 8(a) shows the SEM image of the in situ-synthesized PVA–Fe_3O_4 nanocomposite to confirm the presence of Fe_3O_4 in the polymer matrix. The image also shows a flat surface of pure PVA parts. Fig. 8(b) illustrates the surface of the ex situ-synthesized PVA–Fe_3O_4 nanocomposite, showing a suitable dispersion of Fe_3O_4 in the polymer matrix. In the in situ-synthesized nanocomposites, polymeric chains surround and cover the Fe_3O_4 nanoparticles, and the nanofillers are difficult to observe. However, in the ex situ-synthesized nanocomposites, the presence of Fe_3O_4 nanoparticles is obvious.

The topographic images forming by AFM of PVA and the synthesized PVA–Fe_3O_4 nanocomposites are depicted in Fig. 9. The pure polymer shows smooth surfaces (Fig. 9(a)). The roughness on the surface of the nanocomposite indicates the presence of nanostructures in the PVA (Fig. 9(b) and (c)).

Fig. 10(a) shows the FTIR spectrum of Fe_3O_4 nanoparticles, and exhibits peaks at 438 and 588 cm^{-1}, corresponding to the Fe—O bond in Fe_3O_4 (Ghanbari & Salavati-Niasari, 2015). The absorption peak at 3412 cm^{-1} is the OH groups adsorbed on the surface of nanoparticles. The FTIR spectrum of PVA–Fe_3O_4 nanocomposite is shown in Fig. 10(b). A broad peak occurs at 3300–3400 cm^{-1}, which is related to the O—H bond. An absorption peak at 1729 cm^{-1} is related to the C=O bond in PVA. The peak at 1094 cm^{-1} is attributed to the C—O bonds in PVA. The peak at 2940 cm^{-1} is attributed to the

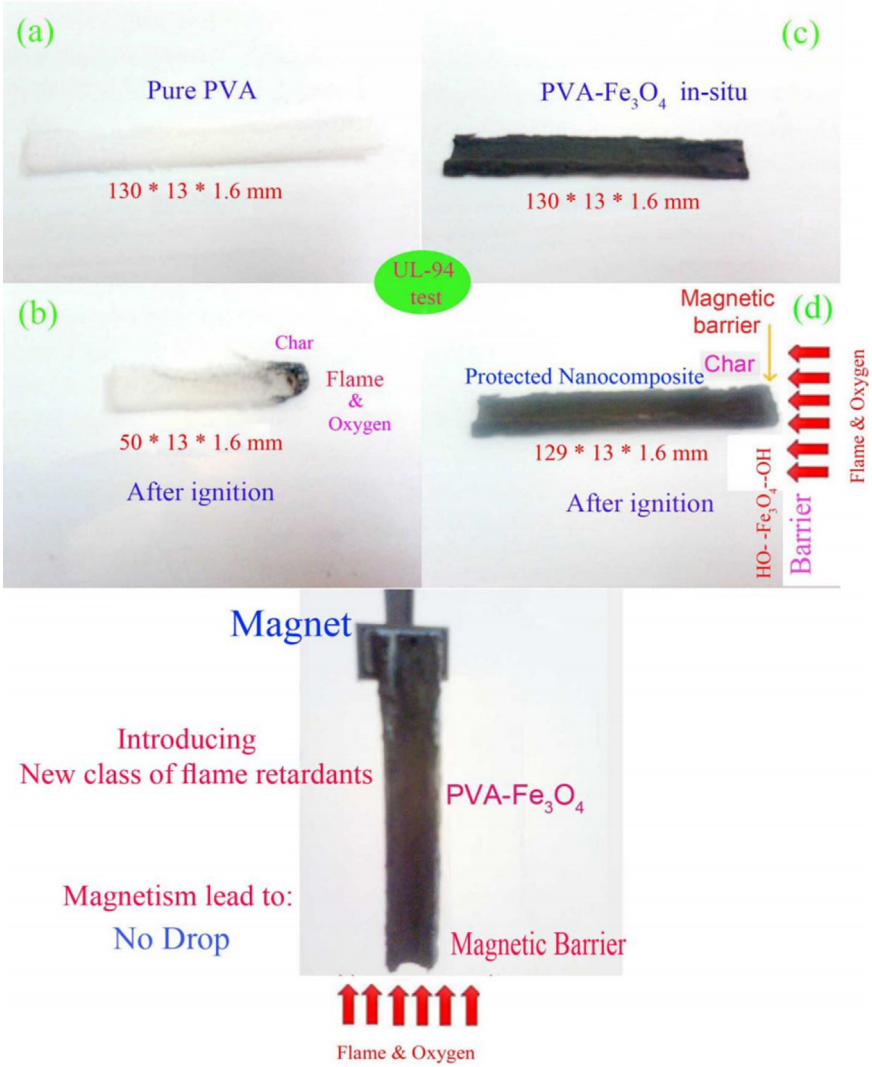

Fig. 14. Comparison of (a, b) pure PVA and (c, d) in situ-synthesized PVA–Fe_3O_4 nanocomposite in the UL-94 test.

Please cite this article in press as: Ghanbari, D., et al. In situ and ex situ synthesis of poly(vinyl alcohol)–Fe_3O_4 nanocomposite flame retardants. *Particuology* (2016), http://dx.doi.org/10.1016/j.partic.2015.12.003

stretching vibration of the C—H bond. The absorptions at 438 and 588 cm^{-1} confirm the presence of nanoparticles in the polymeric nanocomposite.

The hysteresis graph of FeOOH nanoparticles is depicted in Fig. 11(a), showing paramagnetic behavior. Hysteresis loops for Fe_3O_4 nanoparticles is shown in Fig. 11(b). Fe_3O_4 nanoparticles exhibit ferrimagnetic behavior with a saturation magnetization of 48.4 emu/g and a coercivity of 50.2 Oe. Fig. 11(c) shows the hysteresis loop for the PVA–Fe_3O_4 nanocomposite, also exhibiting ferrimagnetic behavior with a saturation magnetization of 7.6 emu/g and a coercivity of 114 Oe.

The PVA–Fe_3O_4 nanocomposite magnetization (defined as the magnetic moment per unit gram) is much lower than (about one fifth of) that obtained for Fe_3O_4 nanoparticles. This magnetization value is rational because of the preparation of nanocomposite is 1 g of magnetite to 4 g of PVA. The results indicate that forming the nanocomposite and distributing Fe_3O_4 into the PVA results in an increase in the coercivity. The magnetic moments of Fe_3O_4 nanoparticles are shielded by the polymer chains, consequently, a higher magnetic field is required to align the single domain nanoparticles in the field direction. A schematic of distribution of Fe_3O_4 nanoparticles in the PVA matrix and their resistance in presence of a magnetic field is shown in Fig. 12 (Ghanbari & Salavati-Niasari, 2015; Ghanbari et al., 2014).

The thermal stabilities of the pure PVA and PVA–Fe_3O_4 nanocomposite were investigated by TGA, and the curves are shown in Fig. 13(a) and (b), respectively. Because of the presence of Fe_3O_4, the thermal decomposition of the nanocomposite was shifted toward higher temperatures. A schematic of the potential interactions (hydrogen bonding) between OH adsorbed on the surface of nanoparticles and hydroxyls of PVA is shown in Fig. 13(c). The nanocomposite performance against heat is illustrated in Fig. 13(d). The dispersed Fe_3O_4 nanoparticles can act as a barrier to slow product volatilization and thermal transport during decomposition of the nanocomposite.

The influence of Fe_3O_4 on flame retardancy was evaluated using the UL-94 test. If the sample was extinguished in less than 10 s after any flame application, the result is classified as V-0. Drips of particles are allowed if they are not inflamed. Samples are ranked as N.C. in UL-94 tests when the maximum total flaming time is above 50 s (Jamshidi, Ghanbari, & Salavati-Niasari, 2014).

The outcomes of the UL-94 tests for PVA, ex situ and in situ-synthesized PVA–Fe_3O_4 were N.C, V-0, and V-0, respectively. The results show that the addition of Fe_3O_4 can enhance the flame retardancy of the PVA matrix. According to the UL-94 test, Fe_3O_4 nanoparticles appropriately interacted with PVA chains to protect the matrix from volatilization. The comparison of pure PVA and in situ-synthesized PVA–Fe_3O_4 nanocomposites in the UL-94 test is shown in Fig. 14.

Nanoparticles can play the role of a barrier layer. This magnetic barrier layer precludes oxygen from reaching the sample. The in situ-synthesized PVA–Fe_3O_4 nanocomposite shows a better performance compared with that of the ex situ-synthesized nanocomposite because the residual chlorine and ammonia have a role in flame retardancy. Hydroxyl groups on the surface of Fe_3O_4 have suitable interactions with hydroxyl groups of PVA, and the Fe_3O_4 nanoparticles have good dispersion in the polymer matrix. In the presence of a flame and occurrence of polymer decomposition, the magnetic nanoparticles remain together, show resistance to dripping and build a barrier. This obstruction slows the evaporation of polymeric segments and prevents the product from heat and flame (Ghanbari et al., 2012; Ghanbari, Salavati-Niasari, & Sabet, 2013; Jamshidi et al., 2014; Yousefi, Noori, Ghanbari, Salavati-Niasari, & Gholami, 2014).

Conclusions

Fe_3O_4 nanoparticles were synthesized via a precipitation reaction at room temperature without using an inert atmosphere. Fe_3O_4 Nanoparticles were characterized using XRD, SEM, TEM, EDS, and AFM techniques. The effects of different parameters such as precursor and reducing agent on the morphology of the products were investigated. The Fe_3O_4 nanoparticles exhibit ferrimagnetic behavior with a saturation magnetization of 48.4 emu/g and a coercivity of 50.2 Oe at room temperature. Coercivity was increased by the formation of the nanocomposite and distribution of the Fe_3O_4 into PVA. The results show that these nontoxic nanofillers improve the thermal stability and flame retardancy of the PVA matrix.

Acknowledgments

Authors are grateful to the council of Iran National Science Foundation (91053846) and University of Kashan for supporting this work by Grant No. (159271/979).

References

Beyer, G. (2001). Flame retardant properties of EVA-nanocomposites and improvements by combination of nanofillers with aluminium trihydrate. *Fire and Materials*, *25*(5), 193–197.
Franco, C. A., Nassar, N. N., & Cortés, F. B. (2014). Removal of oil from oil-in-saltwater emulsions by adsorption onto nano-alumina functionalized with petroleum vacuum residue. *Journal of Colloid and Interface Science*, *433*, 58–67.
Ghanbari, D., & Salavati-Niasari, M. (2015). Synthesis of urchin-like CdS-Fe_3O_4 nanocomposite and its application in flame retardancy of magnetic cellulose acetate. *Journal of Industrial and Engineering Chemistry*, *24*, 284–292.
Ghanbari, D., Salavati-Niasari, M., & Ghasemi-Kooch, M. (2014). A sonochemical method for synthesis of Fe_3O_4 nanoparticles and thermal stable PVA-based magnetic nanocomposite. *Journal of Industrial and Engineering Chemistry*, *20*(6), 3970–3974.
Ghanbari, D., Salavati-Niasari, M., & Sabet, M. (2013). Preparation of flower-like magnesium hydroxide nanostructure and its influence on the thermal stability of poly vinyl acetate and poly vinyl alcohol. *Composites Part B: Engineering*, *45*(1), 550–555.
Ghanbari, D., Salavati-Niasari, M., & Sabet, M. (2012). Polymeric matrix nanocomposites: Influence of cadmium sulfide nanostructure on the thermal degradation of poly (vinyl alcohol) and cellulose acetate. *Journal of Cluster Science*, *23*(4), 1081–1095.
Gholamian, F., Salavati-Niasari, M., Ghanbari, D., & Sabet, M. (2013). The effect of flower-like magnesium hydroxide nanostructure on the thermal stability of cellulose acetate and acrylonitrile–butadiene–styrene. *Journal of Cluster Science*, *24*(1), 73–84.
Grigsby, W. J., Ferguson, C. J., Franich, R. A., & Russell, G. T. (2005). Evaluation of latex adhesives containing hydrophobic cores and poly (vinyl acetate) shells: Potential to improve poly (vinyl acetate) performance. *International Journal of Adhesion and Adhesives*, *25*(2), 127–137.
Henrist, C., Mathieu, J. P., Vogels, C., Rulmont, A., & Cloots, R. (2003). Morphological study of magnesium hydroxide nanoparticles precipitated in dilute aqueous solution. *Journal of Crystal Growth*, *249*(1), 321–330.
Jamshidi, P., Ghanbari, D., & Salavati-Niasari, M. (2014). Sonochemical synthesis of $La(OH)_3$ nanoparticle and its influence on the flame retardancy of cellulose acetate nanocomposite. *Journal of Industrial and Engineering Chemistry*, *20*(5), 3507–3512.
Karunakaran, C., Dhanalakshmi, R., & Gomathisankar, P. (2010). Photomineralization of phenol on Al_2O_3: Synergistic photocatalysis by semiconductors. *Research on Chemical Intermediates*, *36*(4), 361–371.
Kuljanin, J., Čomor, M. I., Djoković, V., & Nedeljković, J. M. (2006). Synthesis and characterization of nanocomposite of polyvinyl alcohol and lead sulfide nanoparticles. *Materials Chemistry and Physics*, *95*(1), 67–71.
Laoutid, F., Bonnaud, L., Alexandre, M., Lopez-Cuesta, J. M., & Dubois, P. (2009). New prospects in flame retardant polymer materials: From fundamentals to nanocomposites. *Materials Science and Engineering: R: Reports*, *63*(3), 100–125.
Liu, S., Ying, J., Zhou, X., & Xie, X. (2009). Core-shell magnesium hydroxide/polystyrene hybrid nanoparticles prepared by ultrasonic wave-assisted in-situ copolymerization. *Materials Letters*, *63*(11), 911–913.
Morgan, A. B., & Wilkie, C. A. (Eds.). (2007). *Flame retardant polymer nanocomposites*. New Jersey: John Wiley & Sons.
Sun, X., & Xiang, L. (2008). Hydrothermal conversion of magnesium oxysulfate whiskers to magnesium hydroxide nanobelts. *Materials Chemistry and Physics*, *109*(2), 381–385.

Please cite this article in press as: Ghanbari, D., et al. In situ and ex situ synthesis of poly(vinyl alcohol)–Fe_3O_4 nanocomposite flame retardants. *Particuology* (2016), http://dx.doi.org/10.1016/j.partic.2015.12.003

Wang, H., Fang, P., Chen, Z., & Wang, S. (2007). Synthesis and characterization of CdS/PVA nanocomposite films. *Applied Surface Science*, *253*(20), 8495–8499.

Wang, Z. Y., Liu, Y., & Wang, Q. (2010). Flame retardant polyoxymethylene with aluminium hydroxide/melamine/novolac resin synergistic system. *Polymer Degradation and Stability*, *95*(6), 945–954.

Wu, H., Shao, M., Gu, J., & Wei, X. (2004). Microwave-assisted synthesis of fibre-like $Mg(OH)_2$ nanoparticles in aqueous solution at room temperature. *Materials Letters*, *58*(16), 2166–2169.

Yousefi, M., Noori, E., Ghanbari, D., Salavati-Niasari, M., & Gholami, T. (2014). A facile room temperature synthesis of zinc oxide nanostructure and its influence on the flame retardancy of poly vinyl alcohol. *Journal of Cluster Science*, *25*(2), 397–408.

Please cite this article in press as: Ghanbari, D., et al. In situ and ex situ synthesis of poly(vinyl alcohol)–Fe_3O_4 nanocomposite flame retardants. *Particuology* (2016), http://dx.doi.org/10.1016/j.partic.2015.12.003